Tunable viscoelastic collagen/polyethylene glycol composite hydrogels modulate neural and tumor cell behavior in 3D microenvironments

Hexu Zhang[#], Ziyan Chen[#], Runxiang Yao, Yuyun Liang, Chaoyong He, Jing Yang, Houzhi Kang, and Liyang Shi*

ABSTRACT

Three-dimensional (3D) cell culture systems provide a more physiological environment than traditional two-dimensional cultures by better mimicking the complex interactions within the extracellular matrix (ECM). Among the key properties of the ECM, viscoelasticity is essential for regulating cell behaviors, such as proliferation, differentiation, and migration. However, many present 3D culture systems are complex and technically demanding, which limits their broad application. In this study, we developed two hydrogel systems with identical stiffness but distinct viscoelastic properties, designed to serve as ECM-based 3D culture platforms. These hydrogels were constructed through the cross-linking reaction between type I collagen and functionalized polyethylene glycol derivatives, resulting in either reversible (dynamic) or stable (static) network structures. This platform effectively simulated ECM-like mechanical cues, enabling the investigation of viscoelastic effects on both neural and cancer cell responses. Our results demonstrated that dynamic hydrogels, characterized by rapid stress relaxation, enhanced PC12 cell elongation, promoted neural stem cell differentiation, and significantly facilitated the invasiveness and tumorigenic capacity of DU145 cells *in vitro* and *in vivo*. These findings highlight the critical importance of matrix viscoelasticity in modulating cell behavior and underscore the potential of this hydrogel-based system as a versatile and accessible tool for applications in neural tissue engineering, cancer research, and mechanobiology.

Keywords:
3D cell culture; Hydrogel; Collagen; Viscoelasticity; Cell behavior

#Authors contributed equally.

***Corresponding author:**
Liyang Shi,
liysh777@hnu.edu.cn

How to cite this article:
Zhang, H., Chen, Z., Yao, R., *et al.* Tunable viscoelastic collagen/polyethylene glycol composite hydrogels modulate neural and tumor cell behavior in 3D microenvironments. *Biomater Transl.* 2025, 6(4), 437-449.

doi: 10.12336/bmt.25.00096

1. Introduction

Cells reside within an intricate extracellular microenvironment, which is also defined as the cellular niche.[1] A key non-cellular component of this microenvironment is the extracellular matrix (ECM), which provides physical support and dynamically regulates cell behavior.[2,3] The functional role of the ECM is governed by a combination of biochemical signals and mechanical properties, both of which contribute to its regulatory influence on cellular activities.[4] Notably, the mechanical characteristics of the ECM are crucial for guiding essential cellular behaviors, such as differentiation,[5] migration,[6] and proliferation,[7] through mechanotransduction. To better understand these cellular responses, it is essential to develop biomimetic *in vitro* models that replicate the mechanical characteristics of the ECM. However, traditional two-dimensional cell culture systems fall short in this regard, as they cannot mimic the three-dimensional (3D) topological structure, dynamic mechanical properties, or biochemical gradients present in native ECM.[8,9] As a result, the development of biomimetic ECM models for *in vitro* applications is of significant importance, particularly for drug screening and the investigation of ECM–cell interaction mechanisms. In this context, 3D cell

culture technologies have received increasing attention. These models more accurately mimic the *in vivo* environment, and cells cultured in 3D systems exhibit behaviors and phenotypes that are more physiologically relevant.[10-12]

Hydrogels have been widely employed as platforms for constructing 3D cell culture models due to their excellent biocompatibility and ability to precisely control the critical biophysical and biochemical characteristics of the ECM.[13,14] Through chemical modification, functional groups can be incorporated into the polymer backbone of hydrogels, allowing fine-tuning of their physical and biological properties to simulate various tissue environments.[15] Over the past two decades, numerous studies have revealed that modulating stiffness can greatly influence cell spreading, proliferation, migration, and differentiation.[16,17] While ECM stiffness has been extensively studied, the native ECM also exhibits dynamic mechanical properties, including viscoelasticity.

Viscoelasticity refers to the time-dependent mechanical behavior of a material that exhibits an immediate elastic response, typical of solids, and delayed stress relaxation or energy dissipation, characteristic of viscous fluids.[17] This property more closely resembles the natural ECM and acts as an essential modulator of cell behavior and fate.[18,19] For instance, Roth *et al.*[20] designed a hydrogel with stress-relaxation capabilities to match brain–matrix viscoelasticity. By tuning the relaxation time, they investigated how viscoelasticity affects neural cell development, providing a highly biomimetic *in vitro* model for studying neurodevelopmental disorders. Similarly, Lu *et al.*[21] developed a light-responsive hydrogel that enabled spatiotemporal control of viscoelasticity. This system effectively recapitulated the dynamic mechanical environment of the ECM and offered new insights into cancer cell migration and dissemination. From a 3D bioprinting perspective, Duan *et al.*[22] formulated a series of tissue-matched viscoelastic hydrogels, significantly enhancing cell viability and performance following printing, thereby advancing applications in tissue engineering and regenerative therapies. Despite the recognized importance of ECM viscoelasticity in cell morphogenesis, many present 3D culture systems remain technically complex and challenging to implement, limiting their broader application in cellular studies. Therefore, there is a pressing need for simpler and more accessible systems that can effectively mimic ECM viscoelasticity and facilitate further research in this field.

Collagen, the most abundant structural protein in animals, is a principal ECM constituent. Its unique triple-helical molecular structure provides exceptional mechanical strength, elasticity, and stability, while also contributing to its excellent biocompatibility.[23,24] In the context of 3D cell culture, collagen plays a crucial role by providing integrin-binding motifs and adhesive domains that facilitate cell attachment, spreading, proliferation, and lineage-specific differentiation.[25] Moreover, the propensity of collagen molecules to self-assemble into a porous, fibrillar 3D network closely mimics the topography and architecture of native ECM, offering a physiologically relevant microenvironment that supports cellular interactions, migration, and tissue morphogenesis.[26] Polyethylene glycol (PEG), in contrast, is a synthetic, hydrophilic polymer renowned for its biological inertness and biocompatibility. PEG exhibits minimal protein adsorption and resists non-specific cell adhesion, making it an ideal candidate for creating defined and tunable microenvironments. Importantly, the chemical structure of PEG allows for facile functionalization with reactive groups, such as acrylates, maleimides, or thiols, thereby enabling the development of customized hydrogel systems with precise control over mechanical properties, degradability, and bioactive ligand presentation.[27] By adjusting PEG's cross-linking density, chain length, or reactive chemistry, the physical characteristics of the resulting hydrogel and the biological responses of encapsulated cells can be finely modulated.

In this study, we employed a simplified strategy to fabricate two distinct types of collagen–PEG composite hydrogels by combining type I collagen with two chemically different PEG derivatives. This approach yielded either a dynamically cross-linked network, capable of exhibiting viscoelastic behavior through reversible interactions, or a statically cross-linked network, characterized by stable covalent bonds that lack stress-relaxation capacity. These hydrogels served as 3D culture platforms to investigate the influence of ECM viscoelasticity on various cell models, including PC12 cells (neuronal differentiation model), neural stem cells (NSCs), and prostate cancer DU145 cells. Using these platforms, we investigated how the mechanical dynamics of the ECM, specifically its time-dependent stress-relaxation behavior, influenced cell morphology, proliferation, lineage commitment, and tumor cell migration, thereby advancing our understanding of cell–matrix interactions under more physiologically relevant conditions.

2. Materials and methods

2.1. Preparation of collagen–PEG composite hydrogels

Type I collagen (>300 kDa) was purchased from DB Wuderegen (China) and solubilized in 0.25 M acetic acid. To obtain a collagen solution at the target concentration, 2 M sodium hydroxide was added to the collagen solution until the pH reached 7, yielding a neutralized collagen solution at 6 mg/mL. The 4-arm PEG–benzaldehyde (PEG–CHO; SINOPEG, China) and 4-arm PEG–succinimidyl carbonate (PEG–NHS; SINOPEG, China) powders were separately dissolved in phosphate-buffered saline (PBS) to prepare 12 mg/mL of PEG–CHO and PEG–NHS solutions, respectively. The PEG–CHO or PEG–NHS solution was thoroughly mixed with type I collagen solution at a 1:1 (v/v) ratio. The mixtures were then evenly cast into molds and incubated at 37°C for 30 min to yield hydrogels.

Hunan Research Center of the Basic Discipline for Cell Signaling, College of Biology, Hunan University, Changsha, Hunan, China

2.2. Stiffness, viscoelasticity, and swelling ratios of collagen–PEG composite hydrogels

The mechanical properties of the hydrogels were analyzed using a rotational rheometer (MCR92, Anton Paar, Austria). The prepared hydrogels were placed on the sample testing stage with a PP15 rotor model, and the temperature was set at 25°C. Two testing modes were employed: (i) Dynamic frequency sweep mode, in which a strain of 1% was maintained while scanning frequencies from 0.1 Hz to 1 Hz; (ii) stress relaxation mode, in which a strain of 1% was maintained, and stress relaxation behavior was recorded over a time range of 0.01–1,000 s. The stress relaxation time ($\tau_{1/2}$) was defined as the duration required for the hydrogel's initial stress to decrease to 50%.

The *in vitro* swelling behavior was assessed by monitoring the wet weight of the hydrogels. Specifically, samples were immersed in PBS and retrieved at predetermined time points (0 h; 1–10 days). After retrieval, surface moisture was carefully removed using absorbent paper, and the samples were weighed on an electronic balance. The initial weight at 0 h was recorded as W_0, while the weights at subsequent time points were recorded as W_t. The swelling ratio was calculated using Equation I:

$$\text{Swelling ratio}(\%)=\frac{W_t - W_0}{W_0}\times 100 \quad \text{(I)}$$

2.3. Cell culture and three-dimensional cell encapsulation experiments

PC12 cells (Procell Biotechnology Co., Ltd., China) and DU145 prostate cancer cells (American Type Culture Collection, United States [USA]) were cultured in RPMI-1640 medium (Gibco, USA) supplemented with 10% fetal bovine serum (FBS; Gibco, USA). NSCs were isolated from the cerebral cortex of neonatal Sprague–Dawley rats. Brain tissue was digested with 0.125% trypsin (Gibco, USA) for 18 min, and digestion was terminated by adding 10% FBS. The cell suspension was then passed through a 100 μm cell strainer (Sorfa, China) and centrifuged at 500 × g for 5 min. The resulting cell pellet was cultured in proliferation medium (Table S1) until neurospheres formed.

To identify NSCs, neurospheres were maintained in proliferation medium for 5 days. For adhesion culture, 48-well plates were pretreated with 200 μL of cell adhesion solution (Applygen, China) per well. After centrifugation at 300 × g for 5 min, neurospheres were resuspended in NSC adhesion medium (Table S2) and seeded into the pretreated plates. For single-cell preparation, neurospheres were resuspended in 0.125% trypsin at 37°C for 18 min. Digestion was terminated by adding 10% FBS, and the mixture was passed through a 40 μm cell strainer (Sorfa, China). Subsequently, single cells were centrifuged at 500 × g for 5 min, resuspended in NSC adhesion medium, and seeded into the pretreated plates. Finally, neurospheres and single cells were stained with anti-Nestin monoclonal antibody (1:100; 14-5843-82, eBioscience, USA), anti-SRY-box transcription factor 2 antibody (1:500; Ab97959, Abcam, United Kingdom [UK]), and 4',6-diamidino-2-phenylindole (DAPI; D9542, Sigma, USA).

For 3D cell culture, neurospheres were dissociated into a single-cell suspension, centrifuged, and resuspended in the hydrogel solution prepared as described in Section 2.1. After gelation, cell-laden hydrogels were transferred into 12-well plates and cultured in the appropriate medium. Hydrogels containing NSCs were maintained in NSC adhesion medium for 1 day, then switched to NSC differentiation medium (Table S3). The final cell concentrations for PC12 cells, NSCs, and DU145 cells were 8×10^5, 3×10^6, and 5×10^5 cells/mL, respectively.

2.4. Cell viability and cytoskeleton analysis

At designated time points, the cell-laden hydrogels were washed with PBS for 1 min. Subsequently, an adequate volume of Calcein acetoxymethyl ester/propidium iodide solution (Beyotime, China) was added to completely cover the hydrogels. The samples were then incubated at 37°C for 30 min under light-protected conditions to assess cell viability.

For cytoskeleton analysis, both dynamic and static hydrogels were washed twice with PBS, each wash lasting 1 min. Subsequently, 4% paraformaldehyde (Labcoms, USA) was added for fixation at 37°C for 30 min. Next, 0.2% Triton X-100 (Beyotime, China) was applied for permeabilization at room temperature for 1 h. Finally, Actin-Tracker Green-488 (1:200; C2201S, Beyotime, China) and DAPI (1:500) were added and incubated for 30 min.

After staining, all samples were examined using a confocal microscope (LSM 980, Zeiss, Germany). Z-stack scanning was performed with a slice thickness of 2 μm, and images were acquired from random fields of view within the hydrogel.

2.5. Evaluation of neural stem cell differentiation potential

For the evaluation of NSC differentiation potential, immunofluorescence staining and western blot analysis were employed to detect glial fibrillary acidic protein (GFAP) and β-III tubulin (Tuj-1). After permeabilization, the samples were blocked with 5% FBS, followed by overnight incubation at 4°C with mouse anti-GFAP antibody (1:500; MAB360, Sigma-Aldrich, USA) and rabbit anti-Tuj-1 antibody (1:500; ab18207, Abcam, UK). Subsequently, the hydrogels were incubated for 1 h under light-protected conditions with Alexa Fluor 546- or 488-conjugated goat anti-rabbit or anti-mouse immunoglobulin G (1:500; A-11035/A-11001, Invitrogen, USA). The nuclei were stained with DAPI (1:500) for 30 min. Finally, the samples were analyzed using a confocal microscope.

For western blotting, cell-laden hydrogels were digested with collagenase type I (Shanghai Yuanye Bio-Technology Co. Ltd.,

China) after being minced into small fragments and incubated at 37°C for 30 min. The cells were then centrifuged and rinsed with PBS. For cell lysis, radioimmunoprecipitation assay buffer (Beyotime, China), BeyoZonase™ Super Nuclease (Beyotime, China), phenylmethylsulfonyl fluoride (Solarbio, China), and protease inhibitor cocktail (Sangon, China) were added, and the procedure was performed on ice. The proteins were denatured at 100°C for 5 min. The polyvinylidene fluoride membrane (Vazyme, China) was blocked with 5% skimmed milk (Epizyme, USA) and incubated with the appropriate primary antibodies overnight at 4°C. Secondary antibodies were applied for 1 h at room temperature. Protein bands were visualized using chemiluminescent reagents (Thermo Fisher Scientific, USA), and the relative expression levels were quantified using ImageJ software (National Institutes of Health, USA).

The antibodies used in this study included rabbit anti-Lamin B (1:1000; Ab133741, Abcam, UK), mouse anti-Tuj-1 (1:1000), rabbit anti-GFAP (1:1000), and horseradish peroxidase-conjugated secondary antibodies (1:1000; AWS0001a/AWS0002a, Abiowell, China).

2.6. Animal experiments and histology assay

A total of 8 BALB/c nude male mice (5 weeks old) were obtained from Hunan SJT Laboratory Animal Co., Ltd., China, and randomly divided into three groups: Control group (untreated), dynamic hydrogel group, and static hydrogel group. The experiments were conducted in accordance with the protocols approved by the Institutional Animal Care and Use Committee of Hunan University College of Biology (ethics approval number: HNUBIO202401002), in compliance with the European Union Directive (2010/63/EU).

Dynamic and static hydrogel solutions were prepared and kept on ice until use. The prepared solutions were injected subcutaneously at a volume of 100 μL per mouse, whereas the control group received no treatment. Tumor length and width were measured every 4 days beginning 30 days after treatment to monitor tumor growth, and tumor growth curves were plotted using Equation II:

$$\text{Tumor volume } (\text{mm}^3) = \frac{\text{Length} \times \text{Width}^2}{2} \quad \text{(II)}$$

Tumor samples and major organs were collected 85 days after treatment, following perfusion with paraformaldehyde. The tissues were dehydrated in a sucrose gradient, embedded in optimal cutting temperature compound (OCT) (Sakura Finetek, USA), and sectioned into 10 μm slices using a cryostat microtome (RWD Life Science, China). Sections were stained with hematoxylin solution (Servicebio, China) for nuclear staining and eosin solution (Servicebio, China) for cytoplasmic staining.

After staining, the sections were dehydrated through a graded ethanol series, cleared in xylene (Sinopharm Chemical Reagent, China), and mounted with neutral balsam (Solarbio, China). The stained sections were examined and imaged using a digital slide scanning system (Pannoramic MIDI, 3DHISTECH, Hungary).

2.7. Statistical analysis

Each experiment was conducted with at least three independent biological replicates. Raw data were analyzed and visualized using GraphPad Prism version 8.0 (GraphPad Software, USA), and the normality of the data was assessed. Data that were normally distributed ($p>0.05$) were analyzed using an independent two-sample *t*-test. Data that did not meet the normality assumption ($p\leq0.05$) were analyzed using the non-parametric Mann–Whitney U test for intergroup comparisons.

3. Results

3.1. Dynamic and static collagen–PEG composite hydrogels exhibited distinct stress relaxation behaviors

To fabricate dynamically cross-linked hydrogels, the amino groups (–NH_2) of type I collagen were reacted with the aldehyde groups (CHO) of 4-arm PEG–CHO through a Schiff base reaction to form dynamic covalent imine bonds (**Figure 1A**). These imine bonds are reversible under physiological conditions, allowing repeated formation and dissociation through hydrolysis.[28] As a result, the dynamic hydrogels exhibited rapid stress relaxation and continuous internal network reorganization. This plasticity enables the matrix to accommodate cellular shape changes, traction forces, and migratory demands, thereby facilitating cell proliferation and axonal extension. In contrast, static hydrogels were produced by reacting collagen –NH_2 groups with –NHS groups through a succinimidyl ester reaction, yielding stable amide bonds (**Figure 1A**).[29] These covalent bonds are irreversible and form rigid, tightly cross-linked networks. Consequently, static hydrogels lack stress relaxation capacity and cannot dynamically adjust their internal architecture in response to cellular forces. This rigidity imposes mechanical constraints on embedded cells, limiting their ability to spread, proliferate, and extend processes.

To prepare the hydrogels, type I collagen solution was mixed with either PEG–CHO or PEG–NHS solution at a 1:1 (v/v) ratio. Both mixtures remained highly fluid immediately after mixing, exhibiting typical liquid-like behavior. The solutions were incubated in glass vials at 37°C for 30 min. Upon completion of the cross-linking reactions, solid gel-like materials were observed (**Figure 1B**), indicating the successful formation of hydrogels. Neural cells (PC12 cells and NSCs) and prostate cancer cells (DU145) were subsequently encapsulated within the hydrogels. Distinct morphological differences were observed among the embedded cells, further confirming the hydrogel matrix's suitability for supporting 3D cell culture (**Figure 1B**).

Swelling tests revealed that both the dynamic and static hydrogels exhibited swelling ratios below 10% (**Figure 1C**), suggesting minimal water uptake and demonstrating good long-term structural stability. The rheological properties of both hydrogels were then evaluated. As shown in **Figure 1D**, within the measured frequency range, the storage modulus (G') of each hydrogel was significantly higher than the loss modulus (G")—a characteristic of classical gel behavior.

These findings confirm that both hydrogels can maintain a stable 3D network under physiological shear forces. The measured G' value for both hydrogel types was approximately

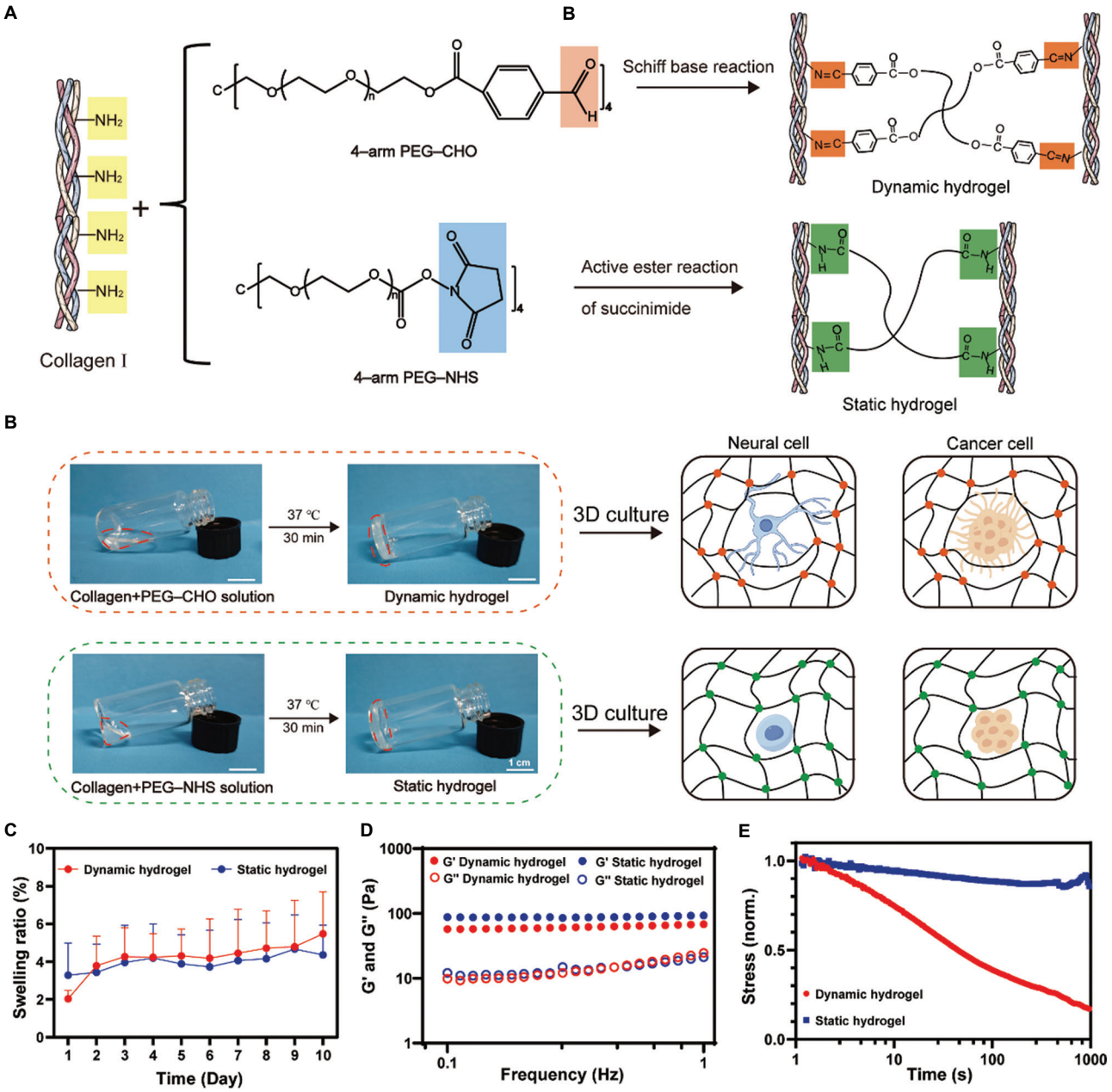

Figure 1. Preparation and characterization of dynamic and static hydrogels. (A) Schematic illustration of the cross-linking mechanisms in dynamic and static hydrogels. (B) Hydrogel formation and representative morphology of encapsulated cells. (C) Swelling ratios of hydrogels ($n = 4$). (D) G' and G" of hydrogels. (E) Stress relaxation behavior of hydrogels.
Abbreviations: 3D: Three-dimensional; Collagen I: Type I collagen; G': Storage modulus; G": Loss modulus; PEG–CHO: 4-arm poly(ethylene glycol)–benzaldehyde; PEG–NHS: 4-arm poly(ethylene glycol)–succinimidyl carbonate.

100 Pa, indicating that, despite differences in cross-linking chemistry, both systems possessed comparable elastic properties. To evaluate the viscoelastic behavior, stress relaxation—defined as the time-dependent reduction in stress at constant strain and considered a typical indicator of viscoelasticity[17,30]—was assessed. As shown in **Figure 1E**, the dynamic hydrogel reached half of its initial stress ($\tau_1/_2$) within 45 s, whereas the static hydrogel showed negligible relaxation, with $\tau_1/_2$ approaching infinity. This finding demonstrates that the dynamic hydrogel exhibited significantly faster stress relaxation, in line with its reversible cross-linking mechanism. A summary of these findings is provided in Table S4.

3.2. Dynamically cross-linked hydrogel networks enhanced axon elongation of PC12 neural cells

Matrix mechanics play a critical role in regulating cellular behavior, particularly in the nervous system, where the ECM provides both structural support and biochemical cues essential for neuronal development and function.[31] To further investigate the influence of ECM viscoelasticity, PC12 cells, derived from rat adrenal gland pheochromocytoma, were employed as a neuronal model to examine the effect of matrix stress relaxation on neuronal behaviors. PC12 cells were encapsulated within either dynamically or statically cross-linked hydrogels and cultured under identical conditions (**Figure 2A**).

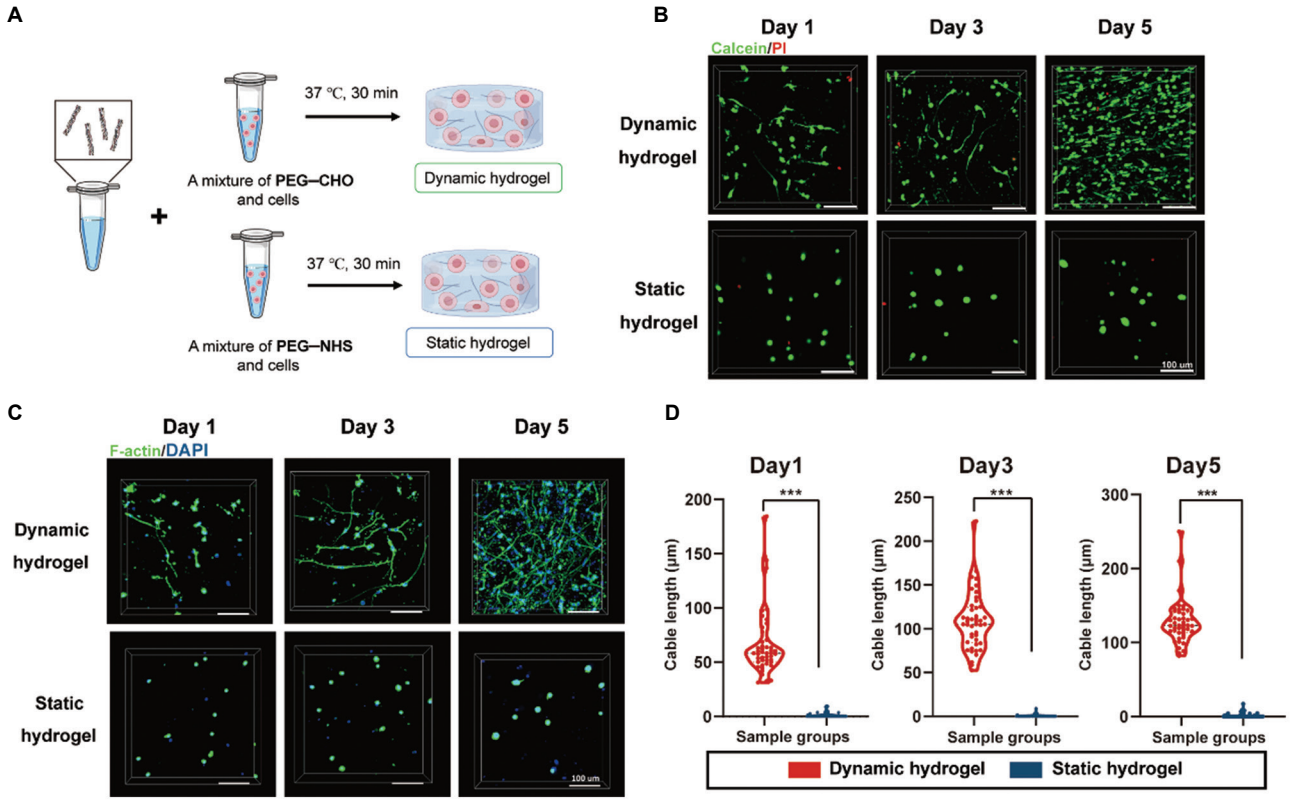

Figure 2. PC12 cell behavior in dynamic and static hydrogels. (A) Schematic illustration of PC12 cell encapsulation within dynamic and static hydrogels. (B) Representative live/dead staining images of PC12 cells (scale bar: 100 μm; magnification: ×400). (C) F-actin immunofluorescence images of PC12 cells encapsulated in hydrogels (scale bar: 100 μm; magnification: ×400). (D) Quantitative analysis of neurite length of PC12 cells cultured in dynamic and static hydrogels (n = 45). Three asterisks (***) indicate statistical significance at $p \leq 0.001$.
Abbreviations: DAPI: 4',6-diamidino-2-phenylindole; F-actin: Filamentous actin; PEG–CHO: 4-arm poly(ethylene glycol)–benzaldehyde; PEG–NHS: 4-arm poly(ethylene glycol)–succinimidyl carbonate; PI: Propidium iodide.

We first assessed cell viability and proliferation. As shown in **Figure 2B**, PC12 cells were uniformly distributed throughout both hydrogel types, with the majority exhibiting green fluorescence in Calcein acetoxymethyl ester/propidium iodide staining, indicating high cell viability in both dynamic and static 3D matrices. Similar viability was observed in cells cultured with either PEG–CHO or PEG–NHS solutions (Figure S1). This observation may be due to the reaction of PEG–CHO and PEG–NHS with $–NH_2$ groups on cell membranes, forming stable chemical bonds without causing cytotoxicity. Furthermore, during the gelation process, the majority of –CHO and –NHS groups were consumed, resulting in hydrogels with excellent biocompatibility. These factors ensure that the chemical reactions involved exerted minimal impact on cellular behavior, thereby supporting the high viability observed in these systems. Key cellular behaviors, such as adhesion, spreading, and neurite outgrowth are tightly regulated by cytoskeletal dynamics, which are known to be influenced by the mechanical properties of the surrounding ECM.[32] To assess how hydrogel cross-linking mechanics affect cytoskeletal remodeling in PC12 cells, we performed fluorescent staining of filamentous-actin (F-actin) using phalloidin. Morphological changes and axonal extension were then analyzed at defined time points post-encapsulation.

As shown in **Figure 2C**, neurite outgrowth was evident as early as day 1 in the dynamic hydrogel, indicating that the viscoelastic matrix provided a favorable environment for initiating neuronal differentiation. The PC12 cells began to extend short neuritic processes, which progressively increased in length and complexity over the course of the culture. With continued incubation, the cells adopted increasingly elongated, spindle-like morphologies—a hallmark of neuronal differentiation[33]—and their axons continued to grow in both length and number. By day 5, the dynamic hydrogel supported the formation of a dense network of interconnected neurites, and the majority of cells exhibited elongated, polarized morphologies with clearly defined neuritic extensions. In stark contrast, PC12 cells encapsulated within the statically cross-linked hydrogel maintained a rounded, compact shape throughout the culture period. Only a limited cytoskeletal rearrangement was observed, and neurite formation was minimal or completely absent. The rigid, non-relaxing matrix appeared to inhibit cellular spreading and the mechanical remodeling necessary for neuronal differentiation and axonal outgrowth.

To quantitatively assess these morphological differences, we measured neurite length under both conditions (**Figure 2D**). The dynamic hydrogel group showed a notable increase in neurite length compared with the static hydrogel group. These findings confirm that the viscoelastic nature of the dynamic hydrogel, characterized by stress-relaxation behavior,

facilitates cytoskeletal reorganization and axonal elongation. Together, these findings suggest that dynamic matrix stress relaxation plays a pivotal role in overcoming the mechanical constraints imposed by the 3D environment. By allowing cells to remodel their surroundings over time, the dynamic hydrogel supports cellular traction forces and cytoskeletal plasticity required for neuronal differentiation and network formation. This highlights the importance of recapitulating native ECM mechanics in biomaterial design for neural tissue engineering and regenerative applications.

3.3. Dynamically cross-linked hydrogel networks promoted neural stem cell differentiation

Neural stem cells are crucial for neurogenesis, possessing the capacity to self-renew and differentiate into various neural lineages, including neurons and astrocytes. Understanding how NSCs respond to different microenvironments is critical for advancing regenerative medicine and neural tissue engineering.[34] In this study, we investigated the behavior of NSCs cultured within dynamically cross-linked hydrogel networks, aiming to assess how matrix viscoelasticity influences their viability and differentiation potential. NSCs were isolated from the brains of neonatal Sprague–Dawley rats, and their stemness was confirmed through standard characterization.

As shown in **Figure 3A**, primary NSCs were cultured in a defined proliferation medium for 5 days, during which time they formed neurospheres. Both the intact neurospheres and the dissociated single cells retained their stem cell characteristics, confirming the high quality and suitability of these cells for subsequent experiments. To assess biocompatibility, we evaluated NSC viability in both dynamic and static hydrogels. As shown in **Figure 3B** and **E**, cell viability in both hydrogel systems exceeded 90% after 1 day of culture and remained above 80% after 3 days. These findings indicate that both hydrogel types support high NSC viability and provide a suitable 3D environment for maintaining metabolic homeostasis. Thus, the dynamic and static hydrogels exhibit excellent cytocompatibility and effectively mimic aspects of the native NSC microenvironment.

Next, we examined how the different cross-linked hydrogel networks regulate NSC differentiation. After 3 days of induction, we assessed the potential of NSCs to differentiate into neurons and astrocytes. As shown in **Figure 3C**, cells cultured in the dynamic hydrogel exhibited distinct morphological features of early-stage neurons and astrocytes. Differentiated neurons displayed elongated neurites, while astrocytes exhibited characteristic multi-branched radial processes, closely resembling their *in vivo* counterparts. In contrast, NSCs cultured in the static hydrogel exhibited weak fluorescence signals and lacked clear neuronal or astrocytic morphology, suggesting limited differentiation. These morphological observations were further supported by immunofluorescence analysis of lineage-specific markers. As shown in **Figure 3D** and quantified in **Figure 3F** and **G**, NSCs in the dynamic hydrogel expressed significantly higher levels of Tuj-1 (a neuronal marker) and GFAP (an astrocyte marker) compared to those in the static hydrogel. These findings indicate that the stress-relaxation behavior of the dynamic hydrogel provides a more favorable mechanical environment for promoting NSC differentiation into neural lineages. In summary, our findings demonstrate that dynamic viscoelastic hydrogels not only maintain high NSC viability but also significantly enhance their neurogenic and gliogenic differentiation potential, highlighting the critical role of matrix mechanics in stem cell fate determination. A summary of these findings is provided in Table S5.

Mechanistically, prior studies support this structure–function relationship. For example, borate-based hydrogels with dynamic stress-relaxation properties have been shown to promote mesenchymal stem cell spreading compared to purely elastic hydrogels, mediated by enhanced yes-associated protein (YAP)/transcriptional coactivator with PDZ-binding motif (TAZ) nuclear localization and altered nuclear morphology.[35] Since YAP activity is tightly regulated by substrate viscoelasticity[36] and interacts with epithelial–mesenchymal transition (EMT) transcription factors, such as zinc finger E-box–binding homeobox 1 to activate transcriptional programmes,[37] this study suggests that similar viscoelastic regulation underlies the enhanced neural proliferation and axonal elongation observed in the dynamic hydrogel system.

3.4. Dynamically cross-linked hydrogel networks influenced the morphology of cancer spheroids *in vitro*

Building on our previous findings regarding the regulation of neural cell behavior by dynamically cross-linked hydrogel networks, we next investigated the response of DU145 prostate cancer cells to these mechanically tunable environments. Given that different cell types exhibit distinct mechanosensitive behaviors, we sought to explore how dynamic matrix properties influence the invasive behavior of DU145 cells, a widely used model for investigating cancer cell invasion and metastasis.[38,39] We first assessed the viability of DU145 cells in both dynamic and static hydrogels. As shown in **Figure 4A**, the cells maintained high viability and stable growth for up to 10 days in both hydrogel types, confirming the biocompatibility of the materials for long-term culture. Similar viability was also observed in cells cultured with PEG–CHO or PEG–NHS solution (Figure S2). Notably, the morphology of DU145 cells evolved differently depending on the mechanical properties of the surrounding matrix. After 3 days of culture, compact multicellular spheroids formed in both hydrogels, serving as a baseline for subsequent morphological transitions. By day 7, spheroids in the dynamic hydrogel exhibited visible cellular protrusions extending from the spheroid periphery, whereas spheroids in the static hydrogel retained smooth, well-defined borders. After 10 days of culture, DU145 spheroids in the dynamic hydrogel lost their compact spherical structure and transformed into irregular aggregates with extensive peripheral spreading. In contrast, spheroids in the static hydrogel remained densely packed and morphologically intact, with minimal signs of cellular invasion.

To further examine cytoskeletal organization and invasive behavior, we performed immunofluorescence staining for F-actin and quantified key morphological parameters, including spheroid size, roundness, and the invasiveness index,

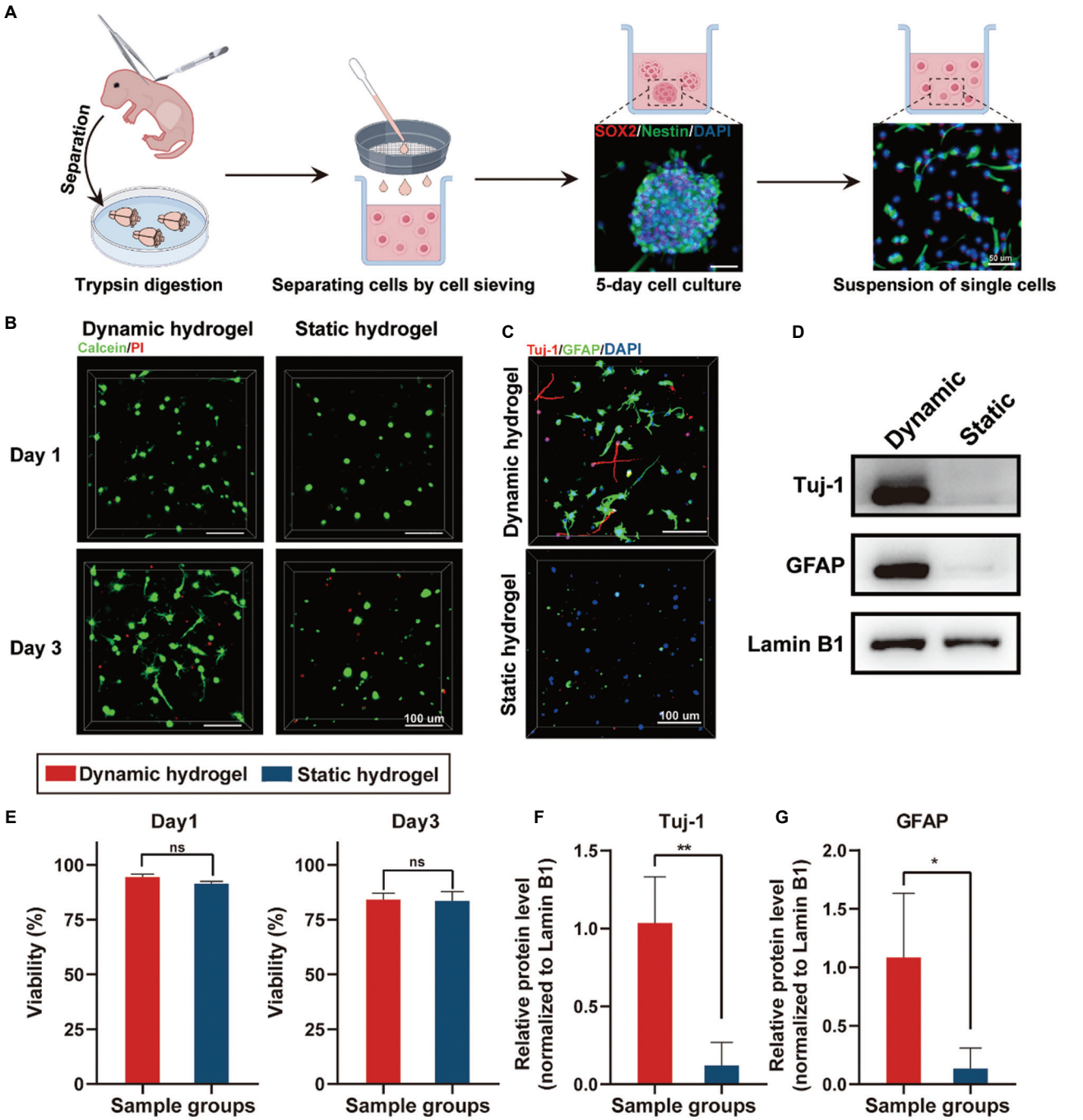

Figure 3. NSC behavior in dynamic and static hydrogels. (A) Schematic illustration of NSC isolation and identification. (B) Representative live/dead staining images of NSCs (scale bar: 100 μm; magnification: ×400). (C) Immunofluorescence images of differentiated NSCs encapsulated in hydrogels, with red indicating Tuj-1 and green representing GFAP (scale bar: 100 μm; magnification: ×400). (D) Protein expression of Tuj-1 and GFAP in NSCs after 3 days of induced differentiation. (E) Quantitative analysis of NSC viability in dynamic and static hydrogels ($n = 3$). (F) Quantitative analysis of Tuj-1 and GFAP protein expression levels by Western blot ($n = 3$). Single asterisk indicates statistical significance at $p \leq 0.05$, double asterisk represents statistical significance at $p \leq 0.01$, and "ns" indicates no statistical significance.

Abbreviations: DAPI: 4',6-diamidino-2-phenylindole; F-actin: Filamentous actin; GFAP: Glial fibrillary acidic protein; Lamin B1: Lamin type B1; PI: Propidium iodide; SOX2: SRY-box transcription factor 2; Tuj-1: β-III tubulin.

a metric reflecting the extent and complexity of peripheral protrusions. By day 3, spheroids had formed in both hydrogels (**Figure 4B**). Quantitative analysis (**Figure 4C**) revealed that the average spheroid diameter in the dynamic hydrogel reached approximately 30 μm, significantly larger than the 18 μm measured in the static hydrogel. By day 7, F-actin–rich cellular protrusions—indicative of increased motility and invasion—were evident at the margins of spheroids in the dynamic hydrogel, while those in the static hydrogel continued to exhibit smooth, non-invasive boundaries. By day 10, protrusive structures in the dynamic group had become more pronounced, suggesting continued invasion into the surrounding matrix (**Figure 4B**).

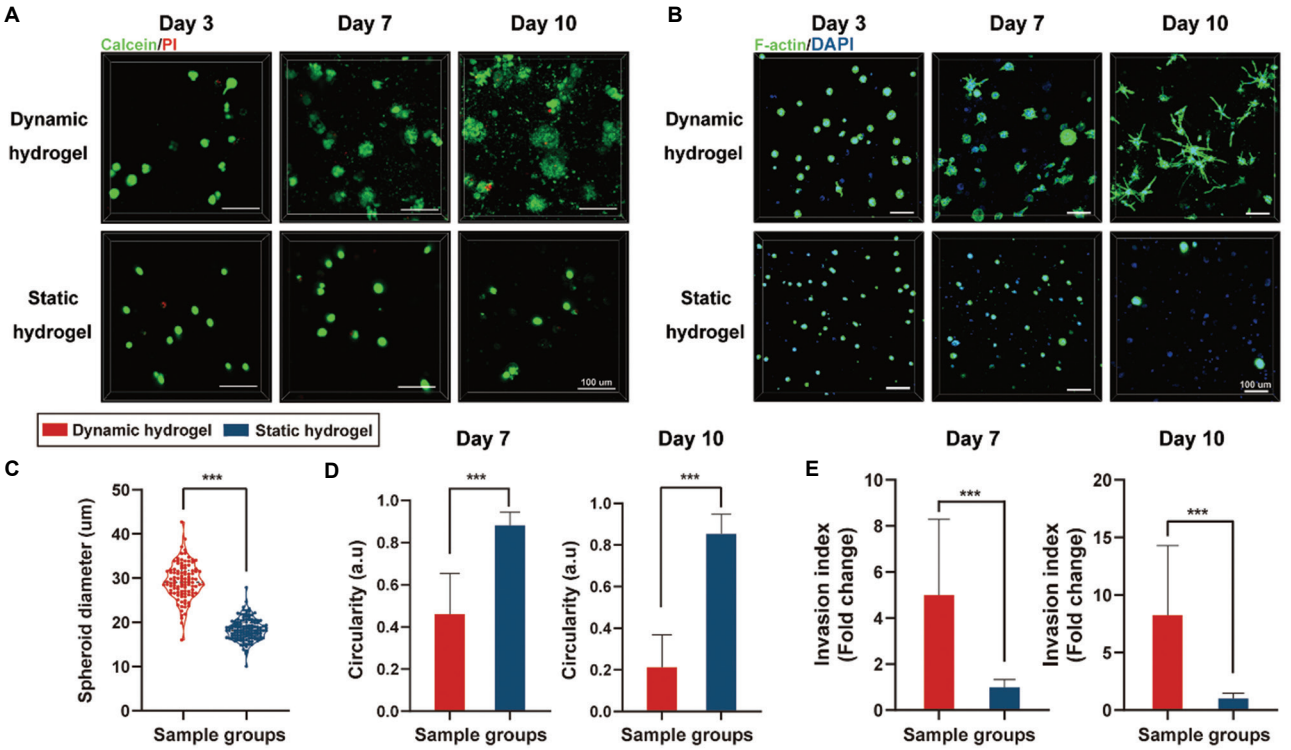

Figure 4. DU145 cell behavior in dynamic and static hydrogels. (A) Representative live/dead staining images of DU145 within hydrogels (scale bar: 100 μm; magnification: ×400). (B) F-actin immunofluorescence images of DU145 cells within hydrogels (scale bar: 100 μm; magnification: ×400). (C) Quantitative analysis of DU145 spheroid diameter after 3 days of treatment in dynamic and static hydrogels (n = 105 for dynamic hydrogel, n =124 for static hydrogel). (D and E) Quantitative analysis of DU145 circularity and invasion index in dynamic and static hydrogels (n = 60). Three asterisks (***) indicate statistical significance at $p \leq 0.001$.
Abbreviations: DAPI: 4',6-diamidino-2-phenylindole; F-actin: Filamentous actin; PI: Propidium iodide.

Spheroid roundness analysis (**Figure 4D**) showed a marked difference between groups: The average roundness index of spheroids in the dynamic hydrogel decreased to below 0.5, indicating significant deviation from a spherical shape. In contrast, spheroids in the static hydrogel retained high roundness values of above 0.8, reflecting their compact and cohesive structure. Furthermore, quantification of the invasiveness index (**Figure 4E**) demonstrated that spheroids in the dynamic hydrogel exhibited significantly higher invasive potential than those in the static hydrogel. Collectively, these results indicate that dynamic hydrogels more effectively promote the transition of DU145 cells toward an invasive phenotype. This was evidenced by enhanced cellular protrusion formation, reduced spheroid roundness, increased heterogeneity in spheroid size and shape, and elevated invasiveness index. Overall, these findings suggest that matrix viscoelasticity plays a key regulatory role in tumor cell behavior and may serve as an important parameter for designing physiologically relevant 3D cancer models.

Saito *et al.*[40] reported that benzaldehyde inhibited the growth of resistant cancer cells by disrupting the interaction of 14-3-3ζ with its client proteins, thereby affecting the transcriptional regulation of EMT- and stemness-related genes. Treatment with a benzaldehyde derivative was shown to inhibit pancreatic tumor growth, reduce lung metastasis, and suppress epithelial–mesenchymal plasticity. In our study, however, DU145 cells encapsulated in both static and dynamic hydrogels exhibited high viability and stable growth over 10 days (**Figure 4A**), indicating good cytocompatibility. More importantly, in dynamic hydrogels containing benzaldehyde-derived imine linkages, DU145 cells displayed enhanced invasive behavior (**Figure 4B**), suggesting that the stress-relaxation dynamics of the matrix played a dominant role in driving invasiveness, rather than any inhibitory effect associated with benzaldehyde groups.

3.5. Dynamically cross-linked hydrogel networks enhanced the tumorigenicity of cancer cells *in vivo*

Given that DU145 cells exhibited enhanced invasive phenotypes within dynamic hydrogels *in vitro*, we next sought to evaluate their tumorigenic potential *in vivo*. A subcutaneous xenograft model was established using BALB/c nude mice. DU145 cells were encapsulated within either dynamic or static hydrogels and implanted subcutaneously into the dorsal region of the mice (**Figure 5A**). Tumor development was monitored over an 85-day period, with tumor volume measured every 4 days. As shown in the tumor growth curve (**Figure 5B**), the dynamic hydrogel group exhibited a significantly faster rate of tumor growth compared to the static hydrogel group. Throughout the study, body weight was also recorded for all mice, and the analysis revealed no significant differences between groups, indicating that the experimental conditions did not affect the overall health of the mice (Figure S3). By day 85, all mice were euthanized through cervical dislocation, and tumor tissues were

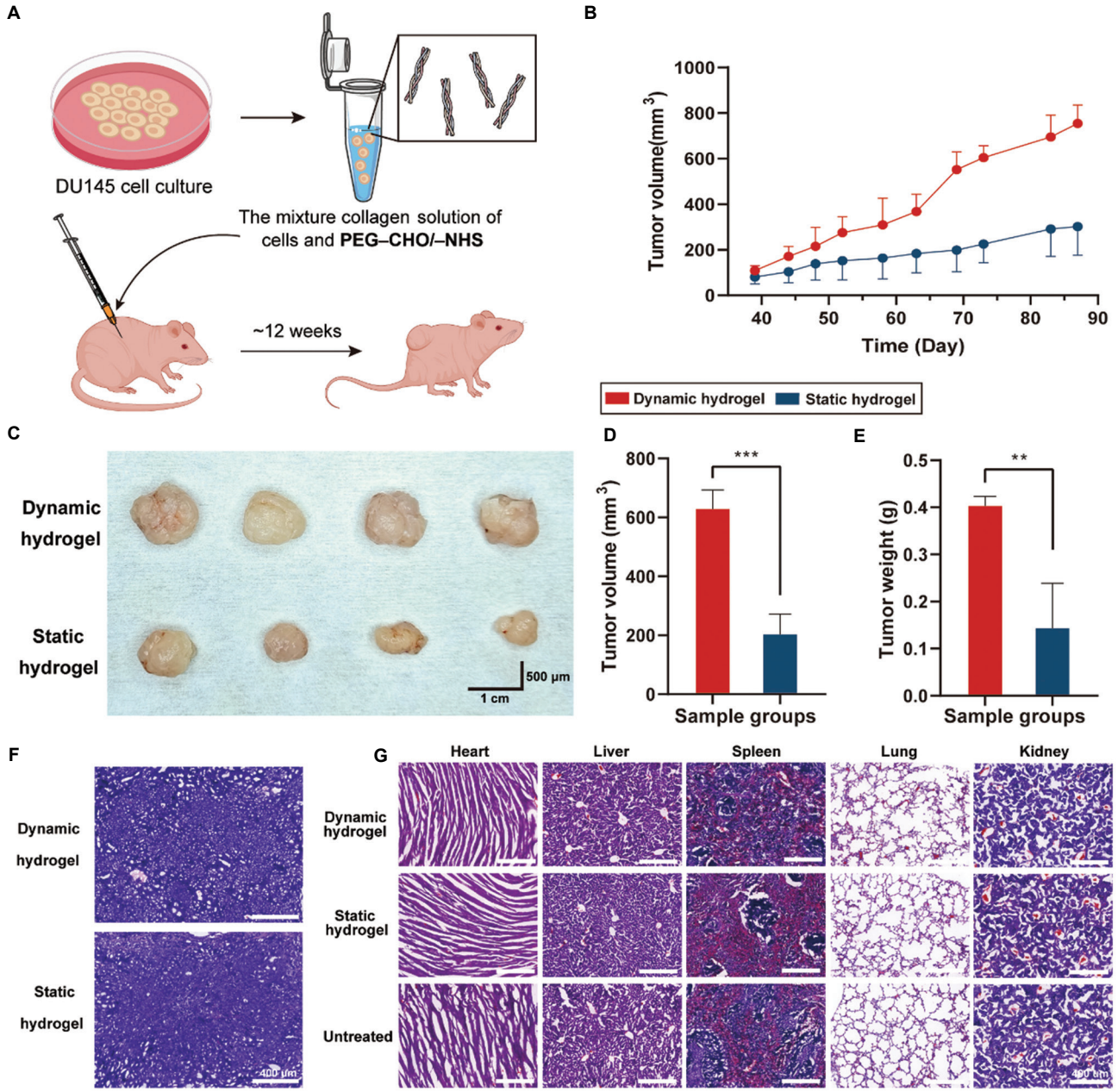

Figure 5. Tumorigenicity of DU145 cells encapsulated in dynamic and static hydrogels *in vivo*. (A) Schematic illustration of subcutaneous tumor-bearing experiment in BALB/c nude mice. (B) Tumor volume growth curves of dynamic and static hydrogel groups ($n = 4$). (C) Representative images of tumors dissected on day 85. (D and E) Tumor volume and weight of dynamic and static hydrogel groups on day 85 ($n = 4$). (F and G) hematoxylin and eosin staining of tumor and major organ tissues on day 85 (scale bar: 400 μm; magnification: ×400). Double asterisk represents statistical significance at $p \leq 0.01$, while three asterisks (***) indicate statistical significance at $p \leq 0.001$.
Abbreviations: PEG–CHO/–NHS: 4-arm poly(ethylene glycol)–benzaldehyde/–succinimidyl carbonate.

carefully excised for further analysis. Gross examination revealed that tumors formed in the dynamic hydrogel group were visibly larger than those in the static group (**Figure 5C**). Quantitative comparison confirmed this observation: Both tumor volume and tumor weight were significantly higher in the dynamic group than in the static group (**Figure 5D** and **E**). These *in vivo* findings were consistent with our *in vitro* results, demonstrating that dynamic viscoelastic hydrogels promote more aggressive growth and enhance the tumorigenicity of DU145 cells.

To assess tissue architecture and cellular morphology, hematoxylin and eosin staining were performed on tumor tissue sections. As shown in **Figure 5F**, tumors from both groups exhibited typical tumor histology, including high cellular density and preserved morphology, confirming successful hydrogel degradation and sustained tumor cell proliferation within the host. Furthermore, to evaluate potential systemic toxicity or off-target effects of the implanted hydrogels, major organs were harvested and subjected to histopathological examination. As shown in **Figure 5G**, the organ tissue sections from both the dynamic and static hydrogel groups displayed normal histological structures, with no detectable pathological changes, comparable to those in untreated control

mice. A summary of these findings is provided in Table S6. Collectively, these findings demonstrate that dynamic hydrogels not only enhance DU145 cell invasiveness *in vitro* but also significantly promote tumor growth *in vivo*, without inducing systemic toxicity.

The viscoelastic properties of the cellular microenvironment are crucial in modulating cell behavior and tumorigenic potential. Previous studies have demonstrated that dynamic stress-relaxing hydrogels promote greater spreading of mesenchymal stem cells compared to purely elastic matrices, primarily through enhanced nuclear localization of YAP/TAZ and consequent changes in matrix remodeling.[35] These alterations in cytoskeletal tension and nuclear morphology directly influence mechanotransduction pathways. Notably, YAP/TAZ activity is tightly associated with EMT, a key process in cancer progression, and has been shown to be regulated by substrate viscoelasticity.[36] Moreover, the EMT transcription factor zinc finger E-box–binding homeobox 1 cooperates with YAP1 to activate oncogenic transcriptional programs, which are particularly prominent in aggressive cancers.[37]

These findings highlight that the dynamic viscoelastic microenvironment of collagen–PEG hydrogels enhances YAP activity and EMT induction in DU145 cells, thereby promoting more invasive phenotypes and stronger tumorigenic growth *in vivo*. Our findings suggest that matrix viscoelasticity is not merely a passive property but an active regulator of tumor progression, providing a mechanistic rationale for the observed differences in DU145 tumorigenicity. Overall, these findings underscore the critical role of ECM viscoelasticity in tumor progression and highlight the potential of dynamic hydrogels as powerful tools for modeling cancer behavior and evaluating therapeutic strategies under physiologically relevant conditions.

4. Discussion

In this study, we successfully constructed dynamic and static hydrogels with distinct network dynamics by integrating type I collagen with functionalized PEG derivatives. These two hydrogel systems served as ECM-based 3D culture platforms to investigate how cross-linking network properties and matrix viscoelasticity influence the behavior of neuronal-like PC12 cells, NSCs, and prostate cancer DU145 cells. Although both hydrogels exhibited comparable stiffness, they demonstrated markedly different viscoelastic behaviors, with the dynamic hydrogel showing a significantly faster stress relaxation rate. These findings highlight that modulation of the cross-linking network's dynamic nature can precisely adjust the viscoelastic properties of hydrogels without altering their bulk stiffness.

Both hydrogel systems demonstrated excellent cytocompatibility with PC12 cells, NSCs, and DU145 cells. However, their effects on cell behavior were notably distinct. The dynamic hydrogel, characterized by a reversible cross-linking network, promoted PC12 cell elongation and neurite outgrowth more effectively, and also enhanced NSC differentiation into neurons and astrocytes compared to the static hydrogel. These findings underscore the critical role of matrix stress relaxation in regulating neural cell morphology, cytoskeletal remodeling, and lineage commitment. These findings suggest that dynamic hydrogels are valuable platforms for investigating neural development and differentiation mechanisms. In addition, their ability to modulate neural cell behavior highlights their potential in regenerative medicine, particularly in the design of biomimetic scaffolds for neural repair and disease modeling in neurodegenerative conditions.

For DU145 cancer cells, *in vitro* experiments revealed that while both hydrogels supported the formation of multicellular spheroids, those cultured in the dynamic hydrogel were significantly larger, less rounded, and developed prominent invasive protrusions over time. Quantitative analyses confirmed that the dynamic hydrogel promoted higher levels of invasiveness. Furthermore, *in vivo* subcutaneous tumorigenesis assays in BALB/c nude mice corroborated these observations: Tumors derived from dynamic hydrogel implants grew more rapidly and reached larger volumes and weights than those in the static hydrogel group. These findings suggest that dynamic matrix properties facilitate not only *in vitro* invasion but also enhance tumorigenic potential *in vivo*. Collectively, these platforms provide physiologically relevant models for investigating tumor progression, invasion mechanisms, and therapeutic resistance. They may also support applications in drug screening and the development of personalized tumor models for precision oncology.

Despite the promising results, the specific molecular mechanisms underlying the observed cell behaviors in dynamic hydrogels remain to be elucidated. Moreover, the chemical reactions used during hydrogel fabrication generate new functional groups, the biological effects of which are not yet fully understood. Future studies employing transcriptomic, proteomic, or mechanotransduction-focused approaches could provide deeper insights into how dynamic viscoelastic properties regulate cell fate and function. In addition, further investigation is warranted to determine whether the reaction byproducts or newly formed chemical groups influence cellular responses. These efforts will be essential for fully understanding the mechanisms of cell–matrix interactions in regenerative medicine and tumor modeling applications.

5. Conclusions

This study successfully demonstrates the potential of dynamic and static hydrogels as versatile ECM-based 3D culture platforms for investigating cell behavior and matrix interactions. By modulating the dynamic nature of the cross-linking network, we achieved precise control over hydrogel viscoelastic properties without altering bulk stiffness, revealing the critical role of matrix stress relaxation in neural cell differentiation and cancer cell invasiveness. The distinct effects of dynamic and static hydrogels on neural and cancer cell behavior underscore their utility in regenerative medicine and oncology research. Future studies focusing on molecular mechanisms and the biological impact of hydrogel fabrication byproducts will further advance our understanding of cell–matrix interactions, paving the way for innovative applications in neural repair, disease modeling, and precision oncology.

Acknowledgement

We thank Professor Dingxiao Zhang from Hunan University for providing DU145 prostate cancer cells and for his invaluable assistance with the animal experiments.

Financial support

This study was financially supported by the Science and Technology Innovation Program of Hunan Province (2024RC3101), the National Natural Science Foundation of China (22275053), the Hunan Provincial Natural Science Foundation of China (2023JJ20005), and the Key Research and Development Program of Hunan Province (2023SK2032).

Conflicts of interest statement

The authors declare no conflict of interest.

Author contributions

Conceptualization: ZC and LS; *Formal analysis*: All authors; *Funding acquisition:* LS; *Investigation:* All authors; *Methodology:* All authors; *Writing – original draft:* HX; *Writing – review & editing:* LS. All authors approved the final version of the manuscript.

Ethics approval and consent to participate

The experiments were conducted in accordance with the protocols approved by the Institutional Animal Care and Use Committee of Hunan University College of Biology (ethics approval number: HNUBIO202401002), in compliance with the European Union Directive (2010/63/EU).

Consent for publication

Not applicable.

Availability of data

Data are available from the corresponding author upon reasonable request.

References

1. Zhang Y, Wang Z, Sun Q, Li Q, Li S, Li X. Dynamic hydrogels with viscoelasticity and tunable stiffness for the regulation of cell behavior and fate. *Materials (Basel).* 2023;16:5161. doi: 10.3390/ma16145161
2. Urbanczyk M, Layland SL, Schenke-Layland K. The role of extracellular matrix in biomechanics and its impact on bioengineering of cells and 3D tissues. *Matrix Biol.* 2020;85-86:1-14. doi: 10.1016/j.matbio.2019.11.005
3. Watt FM, Huck WTS. Role of the extracellular matrix in regulating stem cell fate. *Nat Rev Mol Cell Biol.* 2013;14:467-473. doi: 10.1038/nrm3620
4. Sun B. The mechanics of fibrillar collagen extracellular matrix. *Cell Rep Phys Sci.* 2021;2(8):100515. doi: 10.1016/j.xcrp.2021.100515
5. Kim TH, An DB, Oh SH, Kang MK, Song HH, Lee JH. Creating stiffness gradient polyvinyl alcohol hydrogel using a simple gradual freezing-thawing method to investigate stem cell differentiation behaviours. *Biomaterials.* 2015;40:51-60. doi: 10.1016/j.biomaterials.2014.11.017
6. Doyle AD, Sykora DJ, Pacheco GG, Kutys ML, Yamada KM. 3D mesenchymal cell migration is driven by anterior cellular contraction that generates an extracellular matrix prestrain. *Dev Cell.* 2021;56(6):826-841.e4. doi: 10.1016/j.devcel.2021.02.017
7. Pogoda K, Bucki R, Byfield FJ, *et al.* Soft substrates containing hyaluronan mimic the effects of increased stiffness on morphology, motility, and proliferation of glioma cells. *Biomacromolecules.* 2017;18(10):3040-3051. doi: 10.1021/acs.biomac.7b00324
8. Huang X, Huang Z, Gao W, *et al.* Current advances in 3D dynamic cell culture systems. *Gels.* 2022;8(12):829. doi: 10.3390/gels8120829
9. Urzì O, Gasparro R, Costanzo E, *et al.* Three-dimensional cell cultures: The bridge between *in vitro* and *in vivo* models. *Int J Mol Sci.* 2023;24(15):12046. doi: 10.3390/ijms241512046
10. Ravi M, Paramesh V, Kaviya SR, Anuradha E, Solomon FDP. 3D cell culture systems: Advantages and applications. *J Cell Physiol.* 2015;230(1):16-26. doi: 10.1002/jcp.24683
11. Duval K, Grover H, Han LH, *et al.* Modeling physiological events in 2D vs. 3D cell culture. *Physiology (Bethesda).* 2017;32:266-277. doi: 10.1152/physiol.00036.2016
12. Knight E, Przyborski S. Advances in 3D cell culture technologies enabling tissue-like structures to be created *in vitro*. *J Anat.* 2015;227(6):746-756. doi: 10.1111/joa.12257
13. Xue C, Chen L, Wang N, *et al.* Stimuli-responsive hydrogels for bone tissue engineering. *Biomater Transl.* 2024;5(3):257-273. doi: 10.12336/biomatertransl.2024.03.004
14. Crandell P, Stowers R. Spatial and temporal control of 3D hydrogel viscoelasticity through phototuning. *ACS Biomater Sci Eng.* 2023;9(12):6860-6869. doi: 10.1021/acsbiomaterials.3c01099
15. Lou J, Mooney DJ. Chemical strategies to engineer hydrogels for cell culture. *Nat Rev Chem.* 2022;6:726-744. doi: 10.1038/s41570-022-00420-7
16. Wong SHD, Yin B, Li Z, *et al.* Mechanical manipulation of cancer cell tumourigenicity via heat shock protein signaling. *Sci Adv.* 2023;9(27):eadg9593. doi: 10.1126/sciadv.adg9593.
17. Chaudhuri O, Cooper-White J, Janmey PA, Mooney DJ, Shenoy VB. Effects of extracellular matrix viscoelasticity on cellular behaviour. *Nature.* 2020;584:535-546. doi: 10.1038/s41586-020-2612-2
18. Yang B, Wei K, Loebel C, *et al.* Enhanced mechanosensing of cells in synthetic 3D matrix with controlled biophysical dynamics. *Nat Commun.* 2021;12:3514. doi: 10.1038/s41467-021-23120-0
19. Elosegui-Artola A, Gupta A, Najibi AJ, *et al.* Matrix viscoelasticity controls spatiotemporal tissue organization. *Nat Mater.* 2023;22:117-127. doi: 10.1038/s41563-022-01400-4
20. Roth JG, Huang MS, Navarro RS, Akram JT, LeSavage BL, Heilshorn SC. Tunable hydrogel viscoelasticity modulates human neural maturation. *Sci Adv.* 2023;9(42):eadh8313. doi: 10.1126/sciadv.adh8313
21. Lu Y, Chen C, Li H, *et al.* Visible light-responsive hydrogels for cellular dynamics and spatiotemporal viscoelastic regulation. *Nat Commun.* 2025;16:1365. doi: 10.1038/s41467-024-54880-0
22. Duan Y, Mi X, Yu Q, *et al.* Tailored hydrogels for 3D bioprinting: Matching tissue viscoelasticity to enhance resident cell functionality. *Adv Funct Mater.* 2025:2503987. doi: 10.1002/adfm.202503987
23. Gelse K, Pöschl E, Aigner T. Collagens-structure, function, and biosynthesis. *Adv Drug Deliv Rev.* 2003;55(12):1531-1546. doi: 10.1016/j.addr.2003.08.002.
24. Amirrah IN, Lokanathan Y, Zulkiflee I, Wee MFMR, Motta A, Fauzi MB. A comprehensive review on collagen type I development of biomaterials for tissue engineering: From biosynthesis to bioscaffold. *Biomedicines.* 2022;10(9):2307. doi: 10.3390/biomedicines10092307
25. Sun Q, Hou Y, Chu Z, Wei Q. Soft overcomes the hard: Flexible materials adapt to cell adhesion to promote cell mechanotransduction. *Bioact Mater.* 2021;10:397-404. doi: 10.1016/j.bioactmat.2021.08.026
26. He J, Su Y, Huang T, Jiang B, Wu F, Gu Z. Effects of material and surface functional group on collagen self-assembly and subsequent cell adhesion behaviours. *Colloids Surf B Biointerfaces.* 2014;116:303-308. doi: 10.1016/j.colsurfb.2014.01.009
27. Wang Z, Ye Q, Yu S, Akhavan B. Poly ethylene glycol (PEG)-based hydrogels for drug delivery in cancer therapy: A comprehensive review. *Adv Healthc Mater.* 2023;12(18):2300105.

doi: 10.1002/adhm.202300105

28. Xu J, Liu Y, Hsu SH. Hydrogels based on Schiff base linkages for biomedical applications. *Molecules.* 2019;24(16):3005. doi: 10.3390/molecules24163005
29. Fernandes-Cunha GM, Chen KM, Chen F, *et al. In situ*-forming collagen hydrogel crosslinked via multi-functional PEG as a matrix therapy for corneal defects. *Sci Rep.* 2020;10:16671. doi: 10.1038/s41598-020-72978-5
30. Michida S, Chung UI, Katashima T. Probing the molecular mechanism of viscoelastic relaxation in transient networks. *Gels.* 2023;9(12):945. doi: 10.3390/gels9120945
31. Jain D, Mattiassi S, Goh EL, Yim EKF. Extracellular matrix and biomimetic engineering microenvironment for neuronal differentiation. *Neural Regen Res.* 2020;15(4):573-585. doi: 10.4103/1673-5374.266907
32. Salvi AM, Bays JL, Mackin SR, Mege RM, DeMali KA. Ankyrin G organizes membrane components to promote coupling of cell mechanics and glucose uptake. *Nat Cell Biol.* 2021;23:457-466. doi: 10.1038/s41556-021-00677-y
33. Vieira MS, Santos AK, Vasconcellos R, *et al.* Neural stem cell differentiation into mature neurons: Mechanisms of regulation and biotechnological applications. *Biotechnol Adv.* 2018;36:1946-1970. doi: 10.1016/j.biotechadv.2018.08.002
34. Huang L, Zhang L. Neural stem cell therapies and hypoxic-ischemic brain injury. *Prog Neurobiol.* 2019;173:1-17. doi: 10.1016/j.pneurobio.2018.05.004
35. Tang S, Ma H, Tu HC, Wang HR, Lin PC, Anseth KS. Adaptable fast relaxing boronate-based hydrogels for probing cell-matrix interactions. *Adv Sci.* 2018;5(9):1800638. doi: 10.1002/advs.201800638
36. Zhang J, Yang H, Abali BE, Li M, Xia Y, Haag R. Dynamic mechanics-modulated hydrogels to regulate the differentiation of stem-cell spheroids in soft microniches and modeling of the nonlinear behaviour. *Small.* 2019;15(30):e1901920. doi: 10.1002/smll.201901920
37. Lehmann W, Mossmann D, Kleemann J, *et al.* ZEB1 turns into a transcriptional activator by interacting with YAP1 in aggressive cancer types. *Nat Commun.* 2016;7:10498. doi: 10.1038/ncomms10498
38. Banyard J, Chung I, Migliozzi M, *et al.* Identification of genes regulating migration and invasion using a new model of metastatic prostate cancer. *BMC Cancer.* 2014;14:387. doi: 10.1186/1471-2407-14-387
39. Darnel AD, Behmoaram E, Vollmer RT, *et al.* Fascin regulates prostate cancer cell invasion and is associated with metastasis and biochemical failure in prostate cancer. *Clin Cancer Res.* 2009;15(4):1376-1383. doi: 10.1158/1078-0432.ccr-08-1789
40. Saito J, Onishi N, Yamasaki J, *et al.* Benzaldehyde suppresses epithelial-mesenchymal plasticity and overcomes treatment resistance in cancer by targeting the interaction of 14-3-3ζ with H3S28ph. *Br J Cancer.* 2025;133:27-39. doi: 10.1038/s41416-025-03006-4

Received: July 12, 2025
1st revised: September 16, 2025
2nd revised: September 22, 2025
Accepted: September 23, 2025
Available online: October 17, 2025